

Real-Time Certified Probabilistic Pedestrian Forecasting

Henry O. Jacobs, Owen K. Hughes, Matthew Johnson-Roberson, and Ram Vasudevan

Abstract—The success of autonomous systems will depend upon their ability to safely navigate human-centric environments. This motivates the need for a real-time, probabilistic forecasting algorithm for pedestrians, cyclists, and other agents since these predictions will form a necessary step in assessing the risk of any action. This paper presents a novel approach to probabilistic forecasting for pedestrians based on weighted sums of ordinary differential equations that are learned from historical trajectory information within a fixed scene. The resulting algorithm is embarrassingly parallel and is able to work at real-time speeds using a naive Python implementation. The quality of predicted locations of agents generated by the proposed algorithm is validated on a variety of examples and considerably higher than existing state of the art approaches over long time horizons.

I. INTRODUCTION

Autonomous systems are increasingly being deployed in and around humans. The ability to accurately model and anticipate human behavior is critical to maximizing safety, confidence, and effectiveness of these systems in human-centric environments. The stochasticity of humans necessitates a probabilistic approach to capture the likelihood of an action over a set of possible behaviors. Since the set of plausible human behaviors is vast, this work focuses on anticipating the possible future locations of pedestrians within a bounded area. This problem is critical in many application domains such as enabling personal robots to navigate in crowded environments, managing pedestrian flow in smart cities, and synthesizing safe controllers for autonomous vehicles (AV).

With a particular focus on the AV application several additional design criteria become important. First, false negative rates for unoccupied regions must be minimized. The misclassification of space in this way has obvious safety issues. Second, speed is paramount. To effectively use human prediction within a vehicle control loop prediction rates must be commensurate with the speed at which humans change trajectories. The margins between humans and vehicles are small and both frequently operate at the boundary. Finally, long-time horizon forecasting is preferable since this improves robot predictability, reduces operation close to safety margins, prevents the need for overly conservative or aggressive controllers and makes high-level goal planning more feasible. This paper presents an algorithm for real-time,

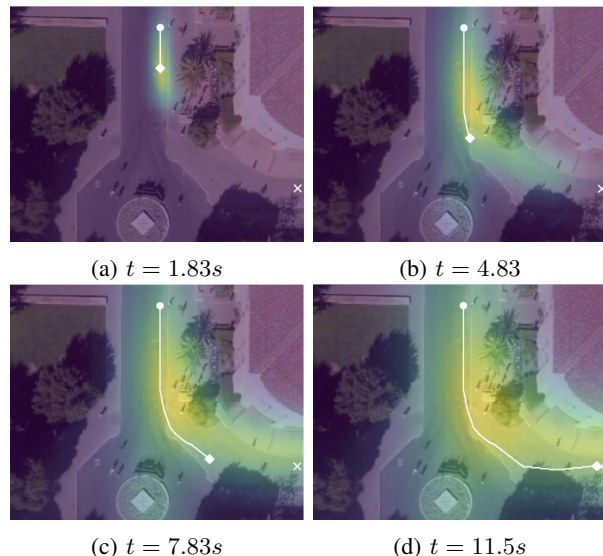


Fig. 1: The performance of the presented algorithm captures the most probable routes that a pedestrian chooses. In this figure, the dot is the start point of the test trajectory, the diamond is the position at time t , and the X is the end of the trajectory. The likelihood of detection is depicted using the *viridis* color palette. In this example which was captured at thirty frames per second, the presented algorithm took 0.00465s per frame in a Python implementation.

long-term prediction of pedestrian behavior which can subsequently be used by autonomous agents. As depicted in Figure 1, this method works quickly to generate predictions that are precise while reducing the likelihood of false negative detections.

A. Background

Most forecasting algorithms are well characterized by the underlying evolution model they adopt. Such models come in a variety of flavors, and are adapted to the task at hand (e.g. crowd modeling [1]). This paper is focused on the construction of useful motion models for pedestrians that can aid the task of real-time forecasting for autonomous agents. The simplest approach to forecasting with motion models forward integrates a Kalman filter [2] based upon the observed heading. Over short time scales this method may perform well, but the resulting distribution devolves into an imprecise Gaussian mass over longer time scales. This is a typical property of the extended Kalman filter and the Kalman filter with deterministic nonlinear drift [3]. In particular, such models are less useful for forecasts beyond two seconds, especially when a pedestrian turns. Nonetheless, these stochastic linear models serve as a reasonable default in the absence of any contextual knowledge. For example,

This work was supported by Ford Motor Company.

H.O. Jacobs, O. Hughes, and R. Vasudevan are with the Department of Mechanical Engineering, University of Michigan, Ann Arbor, MI 48109 {hojacobs, ow Hughes, ramv} @umich.edu

M. Johnson-Roberson is with the Department of Naval and Marine Engineering, University of Michigan, Ann Arbor, MI 48109 mattjr@umich.edu

[4] uses a motion model of this variety, parametrized by latent variables, such as the pedestrian’s awareness of nearby vehicles, to predict when and how a pedestrian may cross a street without leveraging any environmental context.

More sophisticated models that attempt to leverage environmental data include inverse optimal control (IOC) based models [5], [6], [7], [8], [9]. These IOC models have the desirable property of attributing intention and goal-seeking behavior to the agents. For example, [7] extracts a Markov Decision Process (MDP) evolving on a finite 2D lattice by training on a small collection of features and trajectories. The resulting MDP is light-weight since it is parametrized by only a small collection of coefficients equal in number to that of the feature maps. Moreover, given an initial and final state, the probability distribution of the pedestrian at intermediate states is computable using matrix multiplication. The speed of this computation, makes the algorithm of [7] a reasonable baseline for comparison for the algorithm that is presented in this paper.

The approach presented in [7] has been generalized in a variety of ways. For example, time-dependent information, such as traffic signals, are incorporated in [9], by relaxing the Markov property and considering a switched Markov process. Other generalizations in [9] include replacing the finite-state space with a continuous one, and using a Markov jump process in the motion model. Unfortunately the desired posteriors are difficult to compute in closed form, and as a result a sampling based method: a Rao-Blackwellized particle filter [10] is employed. The resulting accuracy of such methods can only be known in a probabilistic sense in that the error bounds are themselves random variables. Moreover, accuracy can come at a large computational expensive which is prohibitive during real-time control.

One limitation of IOC models occurs in cases where there are many locally optimal solutions between a start and end goal. In these cases, IOC type methods can yield non-robust and imprecise behavior. This can occur, for example, when agents make sharp turns due to intermediate criteria on the way toward reaching their final destination. To address this, [11] adopt an empiricists approach, computing “turning maps” and attempting to infer how agents behave in a given patch based on its feature and the behavior of previous agents on similar patches. The motion model is a Markov jump process and the relevant posteriors were approximated using sample based techniques similar to [9]. The objective of [11] is not only prediction, but the development of a motion model learned on one scene that could then subsequently be transferred to other scenes. This requires representations of “objects” in the scene that do not depend rigidly on the finitely many labels an engineer managed to think of in a late-night brainstorming session. For example, such an algorithm should be able to infer how to behave near a roundabout by using prior knowledge of more fundamental building blocks like pavement, curbs, and asphalt.

Along similar lines to [11], [12] constructed an unsupervised approach towards forecasting. As before, the motion model was a Markov jump process, and the training set

was a collection unlabeled videos. Unlike all the approaches mentioned thus far, the agents in [12] were not manually specified. They were learned by detecting which sort of patches of video were likely to move, and how. The resulting predictions outperformed [7] when comparing the most likely path with the ground truth using the mean Hausdorff distance. As in all methods mentioned thus far, computational speed and accuracy of any predicted posteriors were not a concern of [12], so no such results were reported. However, since the motion model was a Markov jump process which required the application of a sample based technique, we should expect the same painful trade-off between error and speed to occur as in [9] and [11].

On the other hand, many authors have approached pedestrian forecasting by deriving their motion model from interactions between pedestrians. Early work by [13] and [14] describe pedestrians interactions using physically motivated methods. Several models such as [15], [16], and [17] derive their motion models from [13] who incorporates collision avoidance through an interaction potential. However this method suffers from not planning for other pedestrian’s positions at future times. [18], [19], and [20] all take optical flow as input. [20] and [18] both use variants of Hierarchical Dirichlet Processes on discretized optical flow to determine temporal motifs (i.e. classes of motion within the scene), where [19] substitutes a Markov model. These models are not agent based, and the lack of an explicit motion model limits their predictive power. [21] predict trajectories by introducing and sampling Anticipatory Temporal Conditional Random Fields which incorporate learned affordances for humans and objects based on observed objectives within the scene. [22], [23], and [24] create agent-based models based on Gaussian Processes, though they suffer issues when trained on discretized trajectories. [25] uses Long Short-Term Memory (Lstm) to learn pedestrian motion models without making assumptions about the manner in which agents will interact and is the state-of-the-art algorithm for socially based models while also having a quick run time.

#1.1

B. Contributions

The primary contributions of this paper are:

- An accurate motion model for pedestrian forecasting.
- An expedient method for computing approximations of relevant posteriors generated by our motion model.
- Hard error bounds on the proposed approximations.

The method proposed by this paper is able to work three times faster than the existing state of the art while improving upon its performance over long time horizons.

For clarification, we should mention that there are a number of things that we do not do. For example, we do not concern ourselves with detection and tracking. Nor do we concern ourselves with updating our prediction as new data comes along [7]. We largely work in a 2D environment with a bird’s eye view, operating under the assumption that the data has been appropriately transformed by a third party. This is in contrast to [9], which operates from first person

video. While it would be a straight forward extension to consider such things, it would detract from the presentation.

The rest of the paper is organized as follows:

- §II describes our motion model as a Bayesian network.
- §III describes how to compute probability densities for an agent's position efficiently.
- §IV demonstrates the model by training and testing it on the Stanford drone dataset [26].

II. MODEL

This paper's goal is to generate a time-dependent probability density over \mathbb{R}^2 , which predicts the true location of an agent in the future. The input to the algorithm at runtime is a noisy measurement of position and velocity, $\hat{x}_0, \hat{v}_0 \in \mathbb{R}^2$. If the (unknown) location of agent at time t is given by $x_t \in \mathbb{R}^2$, then the distribution we seek is the posterior $\rho_t(x_t) := \Pr(x_t | \hat{x}_0, \hat{v}_0)$ for each time $t \in \{\Delta t, \dots, N_t \Delta t\}$ for some user-specified $N_t \in \mathbb{N}$ and $\Delta t \in \mathbb{R}$.

To numerically compute ρ_t , we build a probabilistic graphical model. Our model assumes we have noisy information about agents, and each agent moves with some intention through the world in a way that is roughly approximated by a model. Our model can be divided into three parts:

- 1) Reality: This is parametrized by the true position for all time, x_t , and the initial velocity of the agent v_0 .
- 2) Measurements: This is represented by our sensor readings \hat{x}_0 and \hat{v}_0 and are independent of all other variables given the true initial position and velocity, x_0, v_0 .
- 3) Motion Model: This is represented by a trajectory \tilde{x}_t and depends on a variety of other variables which are described below.

We now elaborate on these three components, and relate them to one another. Many of the choices we make are motivated by a balance between model quality and computational speed (see §III).

A. The Variables of the Model

The model concerns the position of an agent $x_t \in \mathbb{R}^2$ for $t \in [0, N_t \Delta t]$. We denote the position and velocity at time $t = 0$ by x_0 and v_0 respectively. At $t = 0$, we obtain a measurement of position and velocity, denoted by \hat{x}_0 and \hat{v}_0 . Lastly, we have a variety of motion models, parametrized by a set \mathcal{M} (described in the sequel). For each model $m \in \mathcal{M}$, a trajectory \tilde{x}_t given the initial position and velocity x_0 and v_0 . All these variables are probabilistically related to one another in a (sparse) Bayesian network, which we will describe next.

B. The Sensor Model

At time $t = 0$, we obtain a noisy reading of position, $\hat{x}_0 \in \mathbb{R}^2$. We assume that given the true position, $x_0 \in \mathbb{R}^2$, that the measurement \hat{x}_0 is independent of all other variables and the posterior $\Pr(\hat{x}_0 | x_0)$ is known. We assume a similar measurement model for the measured initial velocity \hat{v}_0 .

C. The Agent Model

All agents are initialized within some rectangular region $D \subset \mathbb{R}^2$. We denote the true position of an agent by x_t . We should never expect to know x_t and the nature of its evolution precisely, and any model should account for its own (inevitable) imprecision. We do this by fitting a deterministic model to the data and then smoothing the results. Specifically, our motion model consists of a modeled trajectory \tilde{x}_t , which is probabilistically related to the true position by x_t via a known and easily computable posterior, $\Pr(x_t | \tilde{x}_t)$.

Once initialized, agents come in two flavors: linear and nonlinear. The linear agent model evolves according to the equation $\tilde{x}_t = x_0 + tv_0$ and so we have the posterior:

$$\Pr(\tilde{x}_t \in A | x_0, v_0, lin) = \int_A \delta(\tilde{x}_t - x_0 - tv_0) d\tilde{x}_t. \quad (1)$$

for all measurable sets $A \subset \mathbb{R}^2$, where $\delta(\cdot)$ denotes the multivariate Dirac-delta distribution. For the sake of convenience, from here on we drop the set A and the integral when defining such posteriors since this equation is true for all measurable sets A . We also assume the posteriors, $\Pr(x_0 | lin)$ and $\Pr(v_0 | lin, x_0)$ are known.

If the agent is of nonlinear type, then we assume the dynamics take the form:

$$n \frac{d\tilde{x}_t}{dt} = s \cdot X_k(\tilde{x}_t) \quad (2)$$

where X_k is a vector-field¹ drawn from a finite collection $\{X_1, \dots, X_n\}$, and $s \in \mathbb{R}$. More specifically, we assume that each X_k has the property that $\|X_k(x)\| = 1$ for all $x \in D$. This property ensures that speed is constant in time. As we describe in §IV, the stationary vector-fields X_1, \dots, X_n are learned from the dataset.

It is assumed that k and s are both constant in time, so that \tilde{x}_t is determined from the triple (x_0, k, s) by integrating (2) with the initial condition x_0 . This insight allows us to use the motion model to generate the posterior for $\Pr(\tilde{x}_t | x_0, k, s)$. For each initial condition, x_0 , we can solve (2) as an initial value problem, to obtain a point \tilde{x}_t with initial condition $\tilde{x}_0 = x_0$. This process of solving the differential equation takes an initial condition, \tilde{x}_0 , and outputs a final condition, \tilde{x}_t . This constitutes a map which is termed the *flow-map* [27, Ch 4], and which we denote by $\Phi_{k,s}^t$. Explicitly, we have the posterior:

$$\Pr(\tilde{x}_t | x_0, k, s) = \delta(\tilde{x}_t - \Phi_{k,s}^t(x_0)) d\tilde{x}_t \quad (3)$$

where $\Phi_{k,s}^t$ is the flow-map of the vector field sX_k up to time t . Note that this flow-map can be evaluated for an initial condition efficiently by just integrating the vector field from that initial condition. Note the variables k, s and x_0 determine v_0 . Thus we have the posterior:

$$\Pr(v_0 | k, s, x_0) = \delta(v_0 - sX_k(x_0)) dv_0. \quad (4)$$

¹A vector-field, generally speaking, is an assignment of a velocity to each position in some space. A vector-field on \mathbb{R}^n is nothing but a map from $\mathbb{R}^n \rightarrow \mathbb{R}^n$.

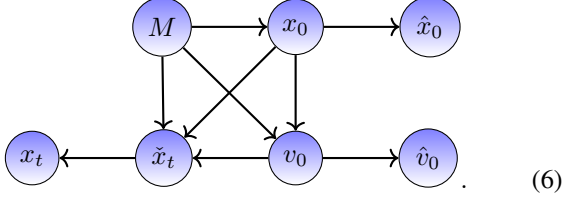
In summary, the agent models are parametrized by the set:

$$\mathcal{M} = \{lin\} \cup (\mathbb{R} \times \{1, \dots, n\}) \quad (5)$$

and each flavor determines the type of motion we should expect from the agent model.

D. The Full Model

Concatenating the measurement model with our motion models yields the Bayesian network, where $M \in \mathcal{M}$ denotes the model of the agent:



We use this Bayesian network to compute ρ_t efficiently. In particular

$$\rho_t(x_t) := \Pr(x_t \mid \hat{x}_0, \hat{v}_0) \quad (7)$$

$$= \left(\sum_k \int \Pr(x_t, k, s \mid \hat{x}_0, \hat{v}_0) ds \right) + \Pr(x_t, lin \mid \hat{x}_0, \hat{v}_0). \quad (8)$$

The final term $\Pr(x_t, lin \mid \hat{x}_0, \hat{v}_0)$ is expressible in closed form when the posteriors $\Pr(x_0 \mid lin)$ and $\Pr(v_0 \mid lin, x_0)$ have known expressions (e.g. Gaussians or uniform distributions). In this instance, the numerical computation of $\Pr(x_t, lin \mid \hat{x}_0, \hat{v}_0)$ poses a negligible burden. Instead the primary computational burden derives from computing $\sum_k \int \Pr(x_t, k, s \mid \hat{x}_0, \hat{v}_0) ds$.

III. EFFICIENT PROBABILITY PROPAGATION

As mentioned, many of the modeling choices are born out of a balance between accuracy and real-time computability. One of the major modeling choices, that agents move approximately according to a small number of ODEs, is the most prominent such choice. This section details how this modeling choice can be leveraged to compute $\rho_t(x_t)$ quickly and accurately.

To begin, rather than focusing on computing $\rho_t(x_t)$, we describe how to compute the joint probability $\Pr(x_t, \hat{x}_0, \hat{v}_0)$. We can obtain $\rho_t(x_t)$ by normalizing $\Pr(x_t, \hat{x}_0, \hat{v}_0)$ with respect to integration over x_t . We can approximate the integration over s in (8), with a Riemann sum. Let us assume that $\Pr(s \mid k)$ is compactly supported for all $k = 1, \dots, n$, and the supported is always contained in some interval $[-\bar{s}, \bar{s}]$ for some $\bar{s} > 0$. Given a regular partition $\{s_0, s_1, \dots, s_n\}$ of step-size $\Delta s > 0$ on $[-\bar{s}, \bar{s}]$, we can conclude that the integral term in (8) can be approximated by

$$\sum_k \int \Pr(x_t, k, s, \hat{x}_0, \hat{v}_0) ds = \underbrace{\Delta s \sum_j \sum_k \Pr(x_t, k, s_j, \hat{x}_0, \hat{v}_0)}_{\text{approximation}} + \underbrace{\varepsilon_s}_{\text{error}} \quad (9)$$

where the error is bounded by $\int |\varepsilon_s| ds \leq TV(x_t, \hat{x}_0, \hat{v}_0) \Delta s$ where $TV(x_t, \hat{x}_0, \hat{v}_0)$ is the sum, with respect to k , of the total variation of $\Pr(x_t, k, s, \hat{x}_0, \hat{v}_0)$ with respect to s for fixed $x_t, \hat{x}_0, \hat{v}_0$. Since this error term can be controlled, the problem of solving $\rho_t(x_t)$ is reduced to that of efficiently computing $\Pr(x_t, k, s_j, \hat{x}_0, \hat{v}_0)$ for a fixed collection of s_j 's.

\hat{x}_0 and \hat{v}_0 are measured and are assumed fixed for the remainder of this section. To begin, from (6) notice that:

$$\Pr(x_t, k, s, \hat{x}_0, \hat{v}_0) = \quad (10)$$

$$= \int \Pr(x_t, \tilde{x}_t, \hat{x}_0, \hat{v}_0, k, s) d\tilde{x}_t \quad (11)$$

$$= \int \Pr(x_t \mid \tilde{x}_t) \Pr(\tilde{x}_t, \hat{x}_0, \hat{v}_0, k, s) d\tilde{x}_t \quad (12)$$

Observe that from the last line that $\Pr(x_t, k, s, \hat{x}_0, \hat{v}_0)$ is a convolution of the joint distribution $\Pr(\tilde{x}_t, \hat{x}_0, \hat{v}_0, k, s)$. Assuming, for the moment, that such a convolution can be performed efficiently, we focus on computation of $\Pr(\tilde{x}_t, \hat{x}_0, \hat{v}_0, k, s)$. Again, (6) implies:

$$\Pr(\tilde{x}_t, \hat{x}_0, \hat{v}_0, k, s) = \quad (13)$$

$$= \int \Pr(\tilde{x}_t, x_0, \hat{x}_0, v_0, \hat{v}_0, k, s) dx_0 dv_0 \quad (14)$$

$$= \int \Pr(\tilde{x}_t \mid x_0, k, s, v_0) \Pr(\hat{v}_0 \mid v_0) \cdot \Pr(v_0 \mid k, s, x_0) \Pr(\hat{x}_0, x_0, k, s) dx_0 dv_0 \quad (15)$$

$$= \int \delta(\tilde{x}_t - \Phi_{k,s}^t(x_0)) \delta(v_0 - sX_k(x_0)) \cdot \Pr(\hat{v}_0 \mid v_0) \Pr(\hat{x}_0, x_0, k, s) dx_0 dv_0, \quad (16)$$

where the last equality follows from substituting (3) and (4). Carrying out the integration over v_0 we observe:

$$\Pr(\tilde{x}_t, \hat{x}_0, \hat{v}_0, k, s) = \int \delta(\tilde{x}_t - \Phi_{k,s}^t(x_0)) \cdot \Pr(\hat{x}_0, x_0, k, s) \Psi(\hat{v}_0; k, s, x_0) dx_0, \quad (17)$$

where $\Psi(\hat{v}_0; k, s, x_0) := \Pr(\hat{v}_0 \mid v_0)|_{v_0=sX_k(x_0)}$. We may approximate $\Pr(\hat{x}_0, x_0, k, s) \Psi(\hat{v}_0; k, s, x_0)$ as a sum of weighted Dirac-delta distributions supported on a regular grid, since $\Pr(\hat{x}_0, x_0, k, s) \Psi(\hat{v}_0; k, s, x_0)$ is of bounded variation in the variable x_0 (with all other variables held fixed).

To accomplish this, let $S_L(\hat{x}_0)$ denote the square of side length $L > 0$ centered around \hat{x}_0 . Choose $L > 0$ to be such that $\int_{S_L(\hat{x}_0)} \Pr(x_0 \mid \hat{x}_0) dx_0 = 1 - \varepsilon_{tol}$ for some error tolerance $\varepsilon_{tol} > 0$. Then, for a given resolution $N_x \in \mathbb{N}$ define the regular grid on $S_L(\hat{x}_0)$ as $\Gamma_L(\hat{x}_0; N_x) := \{x_0^{i,j} \mid i, j \in \{-N_x, \dots, N_x\}\}$, where $x_0^{i,j} = \hat{x}_0 + \frac{L}{2N_x}(i, j)$. The grid spacing is given by $\Delta x = (\frac{L}{2N_x}, \frac{L}{2N_x})$. We approximate the smooth distribution $\Pr(\hat{x}_0, x_0, k, s) \Psi(\hat{v}_0; k, s, x_0)$ as a weighted sum of Dirac-

deltas (in the variable x_0) supported on $\Gamma_L(\hat{x}_0; N)$:

$$\Pr(\hat{x}_0, x_0, k, s) \Psi(\hat{v}_0; k, s, x_0) = \underbrace{\left(\sum_{i,j=-N}^N W(k, s, i, j, \hat{x}_0) \delta(x_0 - x_0^{i,j}) \right)}_{\text{approximation}} + \underbrace{\varepsilon_0(x_0)}_{\text{error}} \quad (18)$$

where $W(k, s, i, j, \hat{x}_0)$ is the evaluation of $\Pr(\hat{x}_0, x_0, k, s) \Psi(\hat{v}_0; k, s, x_0)$ at the grid point $x_0 = x_0^{i,j} \in \Gamma(\hat{x}_0; N)$. More explicitly, this evaluation can be done for each grid point by using only the assumed posterior models in (6). For fixed k and s , the expression $\Pr(\hat{x}_0, x_0, k, s) \Psi(\hat{v}_0; k, s, x_0)$ is a density in x_0 and the error term in (18) has a magnitude of $\|\varepsilon_0\|_{L^1} \sim \mathcal{O}(|\Delta x| + \varepsilon_{tol})$ with respect to the L^1 -norm in x_0 .

Substitution of (18) into the final line of (17) yields:

$$\Pr(\tilde{x}_t, \hat{x}_0, \hat{v}_0, k, s) = \sum_{i,j} W(k, s, i, j, \hat{x}_0) \delta(\tilde{x}_t - \Phi_{k,s}^t(x_0^{i,j})) + \varepsilon_t(\tilde{x}_t) \quad (19)$$

where $\varepsilon_t(\tilde{x}_t) = \int \delta(\tilde{x}_t - \Phi_{k,s}^t(x_0)) \varepsilon_0(x_0) dx_0$. The first term of the right hand side of (19) is computable by flowing the points of the grid, $\Gamma_L(\hat{x}_0; N_x)$, along the vector field sX_k . The second term, ε_t , may be viewed as an error term. In fact, this method of approximating $\Pr(\tilde{x}_t, \hat{x}_0, \hat{v}_0, k, s)$ as a sum of Dirac-delta distributions is adaptive, in that the error term does not grow in total mass, which is remarkable since many methods for linear evolution equations accumulate error exponentially in time [28], [29]:

Theorem 1: The error term, $\varepsilon_t \sim \mathcal{O}(|\Delta x| + \varepsilon_{tol})$ in the L^1 -norm, for fixed k, s, \hat{x}_0 , and \hat{v}_0 . Moreover, $\|\varepsilon_t\|_{L^1}$ is constant in time.

Proof: To declutter notation, let us temporarily denote $\Phi_{k,s}^t$ by Φ . We observe

$$\begin{aligned} \|\varepsilon_t\|_{L^1} &= \int \left| \int \delta(\tilde{x}_t - \Phi(x_0)) \varepsilon_0(x_0) dx_0 \right| d\tilde{x}_t \\ &= \int \det(D\Phi|_{\Phi^{-1}(\tilde{x}_t)}) |\varepsilon_0(\Phi^{-1}(\tilde{x}_t))| d\tilde{x}_t \\ &= \int |\varepsilon_0(u)| du = \|\varepsilon_0\|_{L^1} \end{aligned}$$

As ε_0 is of magnitude $\mathcal{O}(|\Delta x| + \varepsilon_{tol})$ the result follows. ■

While this allows us to compute posteriors over the output of our models, \tilde{x}_t , we ultimately care about densities over the true position. The following corollary of Theorem 1 addresses this:

Corollary 1: The density

$$\sum_{i,j} W(k, s, i, j, \hat{x}_0) \Pr(x_t | \tilde{x}_t)|_{\tilde{x}_t = \Phi_{k,s}^t(x_0^\alpha)} \quad (20)$$

is an approximation of $\Pr(x_t, k, s, \hat{x}_0, \hat{v}_0)$ with a constant in time error bound of magnitude $\mathcal{O}(|\Delta x| + \varepsilon_{tol})$.

Proof: By (12)

$$\Pr(x_t, k, s, \hat{x}_0, \hat{v}_0) = \int \Pr(x_t | \tilde{x}_t) \Pr(\tilde{x}_t, k, s, \hat{x}_0, \hat{v}_0) d\tilde{x}_t$$

Substitution of (18) yields

$$\begin{aligned} \Pr(x_t, k, s, \hat{x}_0, \hat{v}_0) &= \sum_{i,j} W(k, s, i, j, \hat{x}_0) \Pr(x_t | \tilde{x}_t)|_{\tilde{x}_t = \Phi_{k,s}^t(x_0^{i,j})} + \tilde{\varepsilon}_t(x_t) \end{aligned}$$

where the error term is

$$\tilde{\varepsilon}_t(x_t) = \int \Pr(x_t | \tilde{x}_t) \varepsilon_t(\tilde{x}_t) d\tilde{x}_t \quad (21)$$

and ε_t is the error term of (18). We see that the L^1 -norm of $\tilde{\varepsilon}_t$ is

$$\|\tilde{\varepsilon}_t\|_{L^1} = \int \left| \int \Pr(x_t | \tilde{x}_t) \varepsilon_t(\tilde{x}_t) d\tilde{x}_t \right| dx_t \quad (22)$$

$$\leq \int \Pr(x_t | \tilde{x}_t) |\varepsilon_t(\tilde{x}_t)| d\tilde{x}_t dx_t \quad (23)$$

Implementing the integration over x_t first yields:

$$\|\tilde{\varepsilon}_t\|_{L^1} \leq \int |\varepsilon_t(\tilde{x}_t)| d\tilde{x}_t =: \|\varepsilon_t\|_{L^1} \quad (24)$$

which is $\mathcal{O}(|\Delta x| + \varepsilon_{tol})$ by Theorem 1. ■

Corollary 1 justifies using (20) as an approximation of $\Pr(x_t, k, s, \hat{x}_0, \hat{v}_0)$. In particular, this reduces the problem of computing $\rho_t(x_t)$ to the problem of computing the weights $W(k, s, i, j, \hat{x}_0)$ and the points $\Phi_{k,s}^t(x_0^{i,j})$ for all k, s and points $x_0^{i,j} \in \Gamma_L(\hat{x}_0; N_x)$. We can reduce this burden further by exploiting the following symmetry:

Theorem 2: $\Phi_{k,s}^t = \Phi_{k,1}^{st}$.

Proof: Say $x(t)$ satisfies the ordinary differential equation $x'(t) = sX_k(x(t))$ with the initial condition x_0 . In other words, $x(t) = \Phi_{k,s}^t(x_0)$. Taking a derivative of $x(t/s)$, we see $\frac{d}{dt}(x(t/s)) = x'(t/s)/s = X_k(x(st))$. Therefore $x(t/s) = \Phi_{k,1}^t(x_0)$. Substitution of t with $\tau = t/s$ yields $x(\tau) = \Phi_{k,1}^{s\tau}(x_0)$. As $x(\tau) = \Phi_{k,s}^\tau(x_0)$ as well, the result follows. ■

This, allows us to compute $\Phi_{k,s}^t(x_0^\alpha)$ using computations of $\Phi_{k,1}^t(x_0^\alpha)$, which yields the following result:

Theorem 3: Let $\{s_1, \dots, s_n\}$ be a regular partition on the support of $\Pr(s)$. Then the density

$$\begin{aligned} \Delta s \sum_{i,j,k,m} W(k, s_m, i, j, \hat{x}_0) \Pr(x_t | \tilde{x}_t)|_{\tilde{x}_t = \Phi_{k,1}^{s_m t}(x_0^{i,j})} \\ + \Pr(x_t, \text{lin}, \hat{x}_0, \hat{v}_0) \end{aligned} \quad (25)$$

approximates $\Pr(x_t, \hat{x}_0, \hat{v}_0)$ with an error of size $\mathcal{O}(\Delta s + \Delta x + \varepsilon_{tol})$.

Proof: Substitute Theorem 2 into Corollary 1, to replace $\Phi_{k,s}^t$ with $\Phi_{k,1}^{st}$. This gives us an error term of size Δx , if we compute the integral over s exactly. Using (9), we can compute the integral over s approximately, with an error of magnitude Δs . ■

This is a powerful result since it allows us to compute $\Pr(x_t, \hat{x}_0, \hat{v}_0)$ (and thus $\rho_t(x_t)$) at times $t \in \{\Delta t, \dots, N_t \Delta t\}$ with a single computation of $\Phi_{k,1}^{\ell \Delta t s}(x_0^{i,j})$ for each $\ell \in \{-N_t, \dots, N_t\}$, $k \in \{1, \dots, n\}$, and $x_0^{i,j} \in \Gamma_L(\hat{x}_0, N_x)$. To appreciate this, assume we are given

Algorithm 1 Algorithm to compute ρ_t for each $t \in \{\Delta t, 2\Delta t, \dots, N_t \Delta t\}$.

Require: $\bar{s} > 0$, $N_t \in \mathbb{N}$, $\Delta t > 0$, $\{X_k\}_{k=1}^n$, \hat{x}_0 , \hat{v}_0 , $\Gamma_L(\hat{x}_0, N_x)$, $\Pr(x_0 \mid M)$, $\Pr(x_0 \mid \hat{x}_0)$, $\Pr(v_0 \mid \hat{v}_0)$, $\Pr(M \in \mathcal{M})$, and $\Pr(s \mid k)$.

- 1: **for** $\ell \in \{1, \dots, N_t\}$ **do**
- 2: Compute $\Phi_{k,1}^{\pm \bar{s} \ell \Delta t}(x_0^{i,j})$ for all $x_0^{i,j} \in \Gamma_L(\hat{x}_0; N_x)$ and for all $k \in \{1, \dots, n\}$.
- 3: **for** $m \in \{-\ell, \dots, \ell\}$ **do**
- 4: Compute $W(k, s, i, j, \hat{x}_0)$ for $s = \bar{s}m/\ell$ for all $i, j \in \{-N_x, \dots, N_x\}$ and $k \in \{1, \dots, n\}$.
- 5: **end for**
- 6: Compute $\Pr(\check{x}_t, \hat{x}_0, \hat{v}_0)$ at $t = \ell \Delta t$ via Theorem 3 with partition \mathcal{P}_ℓ of (26).
- 7: Apply Bayes' Theorem to obtain $\Pr(\check{x}_t \mid \hat{x}_0, \hat{v}_0)$.
- 8: Compute $\rho_t(x_t)$ at $t = \ell \cdot \Delta t$ via (12).
- 9: **end for**

$\Phi_{k,1}^{m\bar{s}\Delta t}(x_0^{i,j})$ for all $m \in \{-\ell, \dots, \ell\}$. We can then use the regular partition

$$\mathcal{P}_\ell := \left\{ \frac{m}{\ell} \bar{s} \right\}_{m=-\ell}^\ell \quad (26)$$

of $[-\bar{s}, \bar{s}]$ to compute a Riemann sum approximation using Theorem 3. The partition \mathcal{P}_ℓ has a width of size, $\Delta s = \bar{s}/\ell$, and substitution in (25) yields an approximation of $\Pr(x_t, \hat{x}_0, \hat{v}_0)$ at time $t = \ell \Delta t$ given by

$$\frac{\bar{s}}{\ell} \sum_{i,j,k,m} W(k, m\bar{s}/\ell, i, j, \hat{x}_0) \Pr(x_t \mid \check{x}_t) |_{\check{x}_t = \Phi_{k,1}^{m\bar{s}\Delta t}(x_0^{i,j})} + \Pr(x_t, \text{lin}, \hat{x}_0, \hat{v}_0).$$

As we have already computed $\Phi_{k,1}^{m\bar{s}\Delta t}$ for $|m| \leq \ell$ by assumption, the only obstacle to computing this sum is the computation of the weights $W(k, m\bar{s}/\ell, i, j, \hat{x}_0)$. Now if we want to compute $\Pr(x_t, \hat{x}_0, \hat{v}_0)$ at $t = (\ell + 1)\Delta t$, then by reusing the earlier computation one would only need to compute $\Phi_{k,1}^{m\bar{s}\Delta t}(x_0^{i,j})$ for $m \in \{-(\ell+1), (\ell+1)\}$ along with the weights to obtain an approximation using the partition $\mathcal{P}_{\ell+1}$.

The procedure to compute $\rho_t(x_t)$ is summarized in Algorithm 1. For fixed k, i , and j , the computation of $\Phi_{k,1}^t(x_0^{i,j})$ at each $t = \{-N_t \Delta t \bar{s}, \dots, N_t \Delta t \bar{s}\}$ takes $\mathcal{O}(N_t)$ time using an explicit finite difference scheme and can be done in parallel for each $k \in \{1, \dots, n\}$ and $x_0^{i,j} \in \Gamma_L(\hat{x}_0; N_x)$. Similarly, computing $W(k, s, i, j, \hat{x}_0)$ constitutes a series of parallel function evaluations over tuples (k, s, i, j) of the posterior distributions described in (6), where the continuous variable s is only required at finitely many places in Algorithm 1. If the posteriors represented by the arrows in (6) are efficiently computable then the computation of $W(k, s, i, j, \hat{x}_0)$ is equally efficient.

IV. IMPLEMENTATION AND EXPERIMENTAL RESULTS

Given the model established in the previous section, we describe an implementation to showcase one way the

model can be applied to observational data. In particular, we must learn the vector fields $\{X_1, \dots, X_n\}$, the posteriors $\Pr(x_0 \mid M)$ and the priors $\Pr(M)$ for $M \in \mathcal{M}$ from the data. For the purposes of demonstration, we use the Stanford Drone Dataset [26]. More generally, we assume that for a fixed scene we have a database of previously observed trajectories $\{\hat{x}^1, \dots, \hat{x}^N\}$. From this data we tune the parameters of the model ($\{X_1, \dots, X_n\}$, $\Pr(x_0 \mid M)$ and $\Pr(M)$) appropriately.

A. Learning the Vector Fields

We begin by identifying the number of possible vector-fields. To do this we use a clustering algorithm on the trajectories observed in a scene to categorize them into groups. **We then cluster in \mathbb{R}^4 using Affinity Propagation [30] and a custom distance measure defined on the endpoints of trajectories. Let one trajectory A start at $(x_{A,\text{start}}, y_{A,\text{start}})$ and end at $(x_{A,\text{end}}, y_{A,\text{end}})$, and another trajectory B start at $(x_{B,\text{start}}, y_{B,\text{start}})$ and end at $(x_{B,\text{end}}, y_{B,\text{end}})$. We define the points $\mathbf{a}_1 = (x_{A,\text{start}}, y_{A,\text{start}}, x_{A,\text{end}}, y_{A,\text{end}})$, $\mathbf{a}_2 = (x_{A,\text{end}}, y_{A,\text{end}}, x_{A,\text{start}}, y_{A,\text{start}})$, and $\mathbf{b} = (x_{B,\text{start}}, y_{B,\text{start}}, x_{B,\text{end}}, y_{B,\text{end}})$. We then define our distance measure as $d(A, B) := \min \{d_e(\mathbf{a}_1, \mathbf{b}), d_e(\mathbf{a}_2, \mathbf{b})\}$, for the euclidean distance d_e in \mathbb{R}^4 . This function measures the distance between the endpoints irrespective of their ordering, which means that a trajectory that starts from point A and ends at point B will be close to a trajectory that starts from point B and ends at point A. The scale of the datasets we tested on had large enough spatial scale that clustering based on endpoints captured people moving from destination to destination, e.g. from a storefront to the sidewalk at the edge of a scene. On this dataset, distance functions that utilize the entire trajectory such as DTW, LCSS, and PF from [31] and TRACCLUS from [32] did not identify pedestrian intent as well as our method did. While it is unclear why TRACCLUS underperformed on our data, PF, DTW, and LCSS appeared to put trajectories that were very similar for periods of time together even though they had very different intents. This clustering of the end-points induces a clustering of the trajectories. Suppose we obtain clusters S_1, \dots, S_n consisting of trajectories from our data set, as well as a set of unclassified trajectories, S_0 .**

For each set S_k we learn a vector-field that is approximately compatible with that set. Since most trajectories appearing in the dataset have roughly constant speed, we chose a vector-field that has unit magnitude. That is, we assume the vector-field takes the form $X_k(x) = (\cos(\Theta_k(x)), \sin(\Theta_k(x)))$ for some scalar function $\Theta_k(x)$. Learning the vector-fields then boils down to learning the scalar function Θ_k . We assume Θ_k takes the form:

$$\Theta_k(x) = \sum_{\alpha} \theta_{k,\alpha} L_{\alpha}(x),$$

for some collection of coefficients, $\theta_{k,\alpha}$, and a fixed collection of basis functions, L_{α} . In our case, we choose L_{α} to be a set of low degree Legendre polynomials. Θ_k is learned by computing the velocities observed in the cluster, S_k .

These velocities are obtained by a low order finite difference formula. Upon normalizing the velocities, we obtain a unit-length velocity vectors, $v_{i,k}$, anchored at each point, $x_{i,k}$, of S_k . We learn Θ_k by defining the cost-function:

$$C[\Theta_k] = \sum_i \langle v_{i,k}, (\cos(\Theta_k(x_{i,k})), \sin(\Theta_k(x_{i,k}))) \rangle$$

which penalizes Θ_k for producing a misalignment with the observed velocities at the observed points of S_k . When Θ_k includes high order polynomials (e.g. beyond 5th order), we also include a regularization term to bias the cost towards smoother outputs. Using the H^1 -norm times a fixed scalar suffices as a regularization term.

B. Learning $\Pr(x_0 | M)$ and $\Pr(M)$

We first considering the nonlinear models. We begin by assuming that x_0 is independent of s given k , i.e. $\Pr(x_0 | k, s) = \Pr(x_0 | k)$. Additionally, we assume that s and k are independent. This means that we only need to learn $\Pr(x_0 | k)$, $\Pr(k)$, and $\Pr(s)$.

We let $\Pr(k) = (n+1)^{-1}$ and $\Pr(s) \sim \mathcal{U}([-s_{\max}, s_{\max}])$ where $s_{\max} > 0$ is the largest observed speed in the dataset. This implies that $\Pr(\text{lin}) = (n+1)^{-1}$ as well.

For each k we assume $\Pr(x_0 | k) = \frac{1}{Z_k} \exp(-V_k(x_0))$ and V_k is a function whose constant term is 0 and is given by:

$$V_k(x_0; \mathbf{c}) := \sum_{|\alpha| < d} c_\alpha L_\alpha(x_0)$$

for a collection of basis functions, L_α and coefficients $\mathbf{c} = \{c_\alpha\}_{|\alpha| < d}$. We chose our basis functions to be the collection of tensor products of the first six Legendre polynomials, normalized to the size of the domain. Then, one may fit the coefficients c_α to the data by using a log-likelihood criterion. The resulting (convex) optimization problem takes the form:

$$\mathbf{c}^* = \inf_{|\mathbf{c}|} \sum_{x \in S_k} V_k(x_0; \mathbf{c})$$

Where the norm on \mathbf{c} is a sup-norm. We bias this optimization towards more regular functions by adding a penalty to the cost function. Finally, we let $\Pr(x_0 | \text{lin}) \sim \mathcal{U}(D)$.

C. Learning the Measurement Model

We assume a Gaussian noise model. That is

$$\Pr(\hat{x}_0 | x_0) \sim \mathcal{N}(x_0, \sigma_x) \quad , \quad \Pr(\hat{v}_0 | v_0) \sim \mathcal{N}(v_0, \sigma_v).$$

Therefore, our model is parametrized by the standard deviations σ_x and σ_v . We assume that the true trajectory of an agent is smooth compared to the noisy output of our measurement device. This justifies smoothing the trajectories, and using the difference between the smoothed signals and the raw data to learn the variance σ_x . To obtain the results in this paper we have used a moving average of four time steps (this is 0.13 seconds in realtime). We set $\sigma_v = 2\sigma_x/\Delta t$ where $\Delta t > 0$ is the time-step size. This choice is justified from the our use of finite differences to estimate velocity. In particular, if velocity is approximated via finite

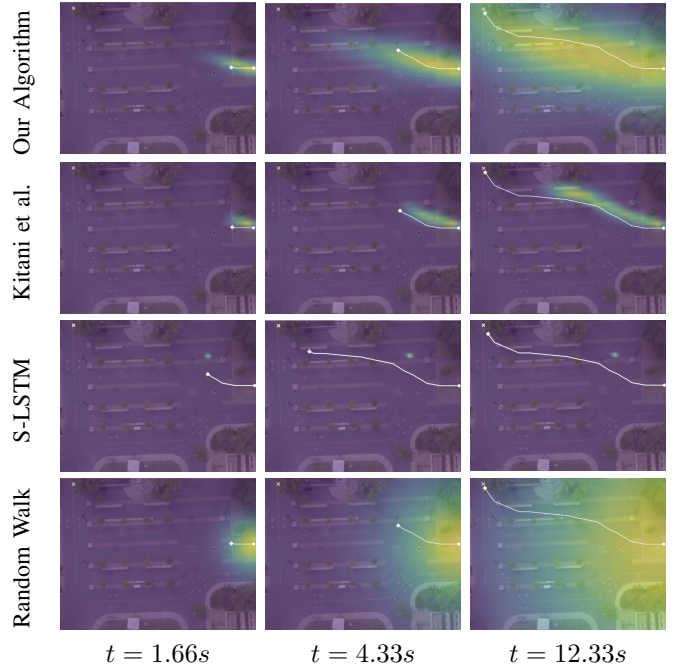


Fig. 2: An illustration of the predictions generated by the various algorithms. In this figure, the dot is the start point of the test trajectory, the diamond is the position at time t , and the X is the end of the trajectory. The likelihood of detection is depicted using the viridis color palette. Notice that the Random Walk is imprecise, while the predictions generated by the algorithm in [7] suffer from the inability of their motion model to adequately match the speed of the agent. The algorithm in [13] is confident and close to the trajectory at small times, but their lack of a motion model causes their prediction to compress into a point at intermediate time scales.

#4.7

differencing as $v(t) \approx (x(t+h) - x(t)) \Delta t^{-1} + \mathcal{O}(h)$ and the measurements are corrupted by Gaussian noise, then the measurement $\hat{v}(t)$ is related to $v(t)$ by Gaussian noise with roughly the same standard deviation as $(x(t+h) - x(t)) \Delta t^{-1}$.

D. Learning the Noise Model

Finally, we assume that the true position is related to the model by Gaussian noise with a growing variance. In particular, we assume $\Pr(x_t | \tilde{x}_t) \sim \mathcal{N}(\tilde{x}_t, \kappa t)$ for some constant $\kappa \geq 0$. The parameter, κ , must be learned. For each curve in S_k we create a synthetic curve using the initial position and speed and integrating the corresponding vector-field, sX_k . So for each curve, $x_i(t)$, of S_k , we have a synthesized curve $x_{i,\text{synth}}(t)$ as well. We then measure the standard deviation of $(x_i(t) - x_{i,\text{synth}}(t))/t$ over i and at few time, $t \in \{0, 100, 200\}$ in order to obtain κ .

E. Evaluating Performance

This section establishes our methods performance and compares it to the model from [7] and a random walk. We implement our model as well as our evaluation code in Python 2.6. Our implementation is available online². We did a 2-fold cross validation by using 20% of the data for testing and the remainder for training within each scene. We learned separate collections of vector fields and model parameters

²https://github.com/OkayHughes/iros2017_pedestrian_forecasting

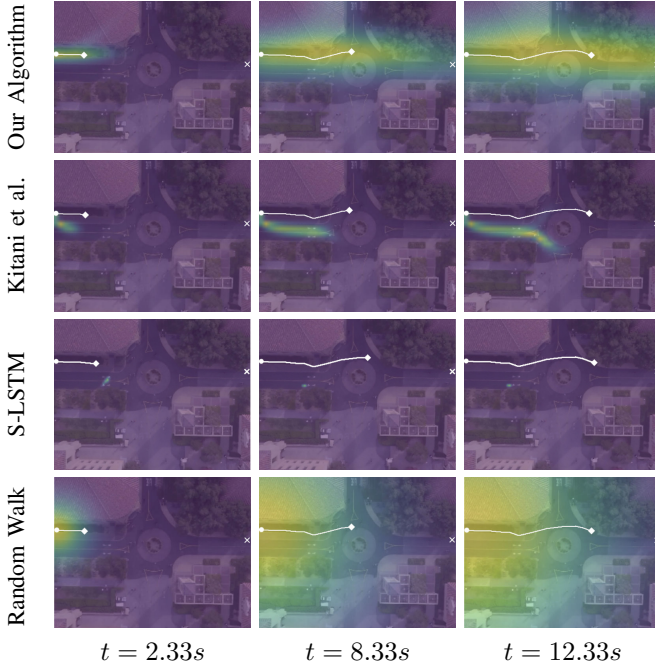


Fig. 3: An illustration of the predictions generated by the various algorithms. In this figure, the dot is the start point of the test trajectory, the diamond is the position at time t , and the X is the end of the trajectory. The likelihood of detection is depicted using the viridis color palette. Notice that the Random Walk is imprecise, while the predictions generated by the algorithm in [7] are unable to match the speed of the agent and choose the wrong direction to follow the agent around the circle. The algorithm in [13] is confident and close to the trajectory at small times, but their lack of a motion model causes their prediction to compress into a point at intermediate time scales.

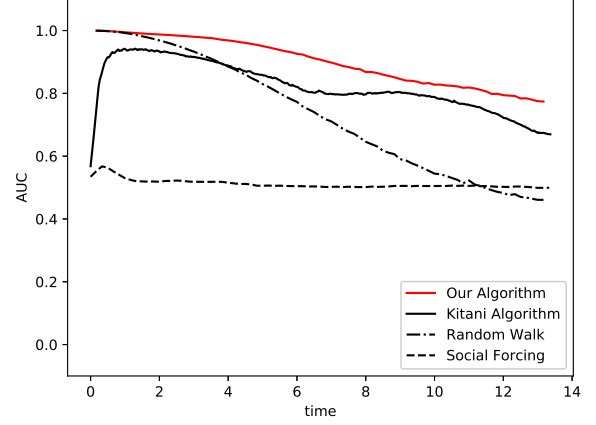


Fig. 4: A comparison of the AUC of the various algorithms. Note that the initial dip in the performance of [7] is due to their confidence in their initial estimate. We sampled the S-LSTM [25] model 100 times in order to give them the best chance in this analysis, but their confidence combined with the over-reliance on outdated pedestrian measurements at moderate-to-large timescales lowered their performance.

TABLE I: Comparison of runtimes of the various algorithms.

	Our Algorithm	Random Walk	Kitani et al.	S-LSTM
time frame	0.00443s	2.1E-7s	0.0706s	0.0134s

for each fold on all of the four scenes on which we tested. Our analysis was conducted on the Coupa, Bookstore, Death Circle, and Gates scenes from the dataset from [26], with a total of 142 trajectories analyzed.

Note that the implementation of the algorithm in [7] required the endpoint of each test trajectory. Without this information the implementation of the predictor provided by the authors devolved into a random walk. Neither our algorithm nor the random walk were provided this information.

The output distributions of the three algorithms were compared using their integrals over the cells of a regular grid over our domain. These integrals are used to visualize the distributions in Figures 2 and 3. Because our predictions all share the same scale, we were able to amalgamate all of the prediction and truth values for all of the simulated agents at a given time step and generate ROC curves. In our analysis, we sought a metric that evaluated the utility of prediction algorithms in the autonomous vehicle context. In this instance it is critical that the generated set of predictions contains the ground-truth observed trajectory while including as few false positive detections as possible. ROC curves which plot the true positive rate (i.e. the proportion of the ground truth trajectory that is correctly identified) against the false positive rate (i.e. the proportion of the generated set that does not correspond to the ground truth trajectory), evaluate this aforementioned safety criteria for autonomous vehicles exactly. The Area Under the Curve (AUC) is a standard

measure of the quality of a predictor. The closer that this AUC is to one, the better the prediction algorithm. Figure ?? shows the analysis of the AUC of each algorithm versus time. In addition, we evaluated the Modified Hausdorff Distance (MHD) from the ground truth trajectory to a sample from the predictions at each time to provide a geometric measure of how accurate the predictions are. Figure ?? shows MHD plotted against time. Though popular in evaluating the geometric proximity of the ground truth trajectory and a predicted set, it is not the most appropriate way to evaluate the utility of an algorithm in the autonomous vehicle context. Specifically consider the instance of a generated set of predictions which does not contain the ground-truth observed trajectory but is close to the ground-truth trajectory geometrically. If this generated set of predictions was used in the autonomous vehicle context, it would not preclude certain portions of the space where the person was occupying. Notice that In this instance the true positive rate would be zero meaning that the generated set of predictions was not useful. Whereas the MHD would describe this generated set of predictions as informative. Our predictor behaves better than any of the other compared methods at moderately large t . This is despite providing the algorithm in [7] with the specific final location of each agent.

The run time per frame for each algorithm was generated using the mean run time for 400 frames, averaged across all of the trajectory data used in the quality analysis. This is shown in Table I. Our algorithm implementation leveraged its embarrassing parallelism using a relatively naive Python im-

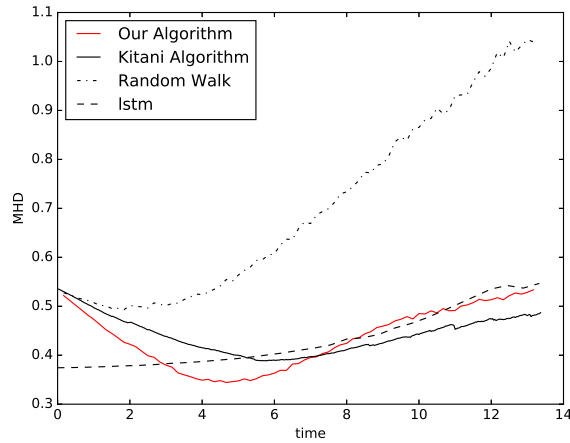


Fig. 5: A comparison of the Modified Hausdorff Distance from the ground truth of the pedestrian to a 1000 point sample from each distribution. The method from [25] does very well at short time scales due to its confidence, but we outperform all other methods at intermediate times. At long timescales the MHD to the trajectory of most algorithms converges. Our method increases positional uncertainty with time, and so [7] outperforms us because they know the end point and we do not, and [25] places too much significance on the initial positions of other pedestrians at large time scales.

plementation, which split the computation of frames among 18 cores. The algorithm in [7] was timed with minimal modification using the source code provided by the authors.

V. CONCLUSION

This paper presents a real-time approach to probabilistic pedestrian modeling. We demonstrate the ability to accurately predict the final location of a pedestrian with superior accuracy compared to a state-of-the-art with additional contributions in three critical areas: 1) prediction speed is efficient enabling tight loop real-time control; 2) our error bound on the predictions accurately reflects potential paths for the human limiting false negatives and maximizing the utility and safety of the predictions; and 3) the prediction made by the proposed approach do not require knowledge of the end point making them applicable to a wide variety of real world applications. These three features have great utility for robotic applications, and we see the integration of such techniques with autonomous system control as one pathway to enable safer operations in shared human-robot spaces. We plan to explore the optimization of the naive python implementation using GPU parallelization to further increase speed and ease integration into system's control loop. Though including social forces into the model is outside of the scope of this paper, its incorporation could begin as follows. In the current motion model with a single vector field, the acceleration of the i th agent is given by $\ddot{x}_i = s^2 DX(x_i) \cdot X(x_i)$. Incorporating a social force F_i acting on the i th agent can be done by instead asserting $\ddot{x}_i = s^2 DX(x) \cdot X(x) + F_i$. Usually $F_i = \sum_j \nabla U(x_j - x_i)$ where U is an interaction potential [13]. The algorithms for generating real-time prediction would then generalize to this new vector-field definition. We also hope to do transfer

learning with this model using scene segmentation from [12], as well as the semantic context descriptors and routing scores from [11] to show how vector fields can be transferred to novel scenes. It appears that the low-order parameterization of our model, and unit-length vector field assumption make it particularly amenable to the methods developed in [11].

ACKNOWLEDGMENTS

Kris Kitani was critical in aiding the comparison to his algorithm.

REFERENCES

- [1] D. Helbing, "A fluid-dynamic model for the movement of pedestrians," *Complex Systems*, vol. 6, pp. 391–415, 1992.
- [2] R. Kalman, "A new approach to linear filtering and prediction problems," *Journal of Basic Engineering*, vol. 82, no. 1, pp. 35–45, 1960.
- [3] N. Schneider and D. M. Gavrilu, "Pedestrian path prediction with recursive bayesian filters: A comparative study," in *Proc. of the German Conference on Pattern Recognition*, 2013.
- [4] *Context-Based Pedestrian Path Prediction*, 2014.
- [5] B. D. Ziebart, A. Maas, J. A. Bagnell, and A. K. Dey, "Maximum entropy inverse reinforcement learning," in *Proc. AAAI*, 2008, pp. 1433–1438.
- [6] B. D. Ziebart, N. Ratliff, G. Gallagher, C. Mertz, K. Peterson, J. A. Bagnell, M. Hebert, A. K. Dey, and S. Srinivasa, "Planning-based prediction for pedestrians," in *IROS*, 2009.
- [7] K. M. Kitani, B. D. Ziebart, J. A. Bagnell, and M. Hebert, *Activity Forecasting*. Berlin, Heidelberg: Springer Berlin Heidelberg, 2012, pp. 201–214.
- [8] D. Xie, S. Todorovic, and S. Zhu, "Inferring "dark energy" and "dark matter" from image and video," in *Proc. Int'l Conference on Computer Vision*, 2013.
- [9] V. Karasev, A. Ayvaci, B. Heisele, and S. Soatto, "Intent-aware long-term prediction of pedestrian motion," *Proceedings of the International Conference on Robotics and Automation (ICRA)*, May 2016.
- [10] A. Doucet, N. d. Freitas, K. P. Murphy, and S. J. Russell, "Rao-blackwellised particle filtering for dynamic bayesian networks," in *Proceedings of the 16th Conference on Uncertainty in Artificial Intelligence*, ser. UAI '00. San Francisco, CA, USA: Morgan Kaufmann Publishers Inc., 2000, pp. 176–183. [Online]. Available: <http://dl.acm.org/citation.cfm?id=647234.720075>
- [11] L. Ballan, F. Castaldo, A. Alahi, F. Palmieri, and S. Savarese, "Knowledge transfer for scene-specific motion prediction," in *Proc. of European Conference on Computer Vision (ECCV)*, Amsterdam, Netherlands, October 2016. [Online]. Available: <http://arxiv.org/abs/1603.06987>
- [12] J. Walker, A. Gupta, and M. Hebert, "Patch to the future: Unsupervised visual prediction," in *Computer Vision and Pattern Recognition*, 2014.
- [13] D. Helbing and P. Molnar, "Social force model for pedestrian dynamics," *Physical review E*, vol. 51, no. 5, p. 4282, 1995.
- [14] Y. Xu and H.-J. Huang, "Simulation of exit choosing in pedestrian evacuation with consideration of the direction visual field," *Physica A: Statistical Mechanics and its Applications*, vol. 391, no. 4, pp. 991–1000, 2012.
- [15] K. Yamaguchi, A. C. Berg, L. E. Ortiz, and T. L. Berg, "Who are you with and where are you going?" in *Computer Vision and Pattern Recognition (CVPR), 2011 IEEE Conference on*. IEEE, 2011, pp. 1345–1352.
- [16] S. Yi, H. Li, and X. Wang, "Pedestrian behavior modeling from stationary crowds with applications to intelligent surveillance," *IEEE transactions on image processing*, vol. 25, no. 9, pp. 4354–4368, 2016.
- [17] S. Pellegrini, A. Ess, K. Schindler, and L. Van Gool, "You'll never walk alone: Modeling social behavior for multi-target tracking," in *Computer Vision, 2009 IEEE 12th International Conference on*. IEEE, 2009, pp. 261–268.
- [18] R. Emonet, J. Varadarajan, and J.-M. Odobez, "Extracting and locating temporal motifs in video scenes using a hierarchical non parametric bayesian model," in *Computer Vision and Pattern Recognition (CVPR), 2011 IEEE Conference on*. IEEE, 2011, pp. 3233–3240.
- [19] T. Hospedales, S. Gong, and T. Xiang, "A markov clustering topic model for mining behaviour in video," in *Computer Vision, 2009 IEEE 12th International Conference on*. IEEE, 2009, pp. 1165–1172.

- [20] X. Wang, X. Ma, and W. E. L. Grimson, "Unsupervised activity perception in crowded and complicated scenes using hierarchical bayesian models," *IEEE Transactions on pattern analysis and machine intelligence*, vol. 31, no. 3, pp. 539–555, 2009.
- [21] H. S. Koppula and A. Saxena, "Anticipating human activities using object affordances for reactive robotic response," *IEEE transactions on pattern analysis and machine intelligence*, vol. 38, no. 1, pp. 14–29, 2016.
- [22] M. Tay and C. Laugier, "Modelling smooth paths using gaussian processes," in *Field and Service Robotics*. Springer, 2008, pp. 381–390.
- [23] J. M. Wang, D. J. Fleet, and A. Hertzmann, "Gaussian process dynamical models for human motion," *IEEE transactions on pattern analysis and machine intelligence*, vol. 30, no. 2, pp. 283–298, 2008.
- [24] P. Trautman, J. Ma, R. M. Murray, and A. Krause, "Robot navigation in dense human crowds: Statistical models and experimental studies of human-robot cooperation," *The International Journal of Robotics Research*, vol. 34, no. 3, pp. 335–356, 2015.
- [25] A. Alahi, K. Goel, V. Ramanathan, A. Robicquet, L. Fei-Fei, and S. Savarese, "Social lstm: Human trajectory prediction in crowded spaces," in *Proceedings of the IEEE Conference on Computer Vision and Pattern Recognition*, 2016, pp. 961–971.
- [26] A. Robicquet, A. Sadeghian, A. Alahi, and S. Savarese, *Learning Social Etiquette: Human Trajectory Understanding In Crowded Scenes*. Cham: Springer International Publishing, 2016, pp. 549–565. [Online]. Available: http://dx.doi.org/10.1007/978-3-319-46484-8_33
- [27] R. Abraham, J. E. Marsden, and T. S. Ratiu, *Manifolds, Tensor Analysis, and Applications*, 3rd ed., ser. Applied Mathematical Sciences. Springer, 2009, vol. 75.
- [28] R. J. LeVeque, *Numerical methods for conservation laws*, 2nd ed., ser. Lectures in Mathematics ETH Zürich. Birkhäuser Verlag, Basel, 1992. [Online]. Available: <http://dx.doi.org/10.1007/978-3-0348-8629-1>
- [29] D. Gottlieb and J. Hesthaven, "Spectral methods for hyperbolic problems," *Journal of Computational and Applied Mathematics*, vol. 128, no. 1–2, pp. 83 – 131, 2001, numerical Analysis 2000. Vol. VII: Partial Differential Equations. [Online]. Available: <http://www.sciencedirect.com/science/article/pii/S0377042700005100>
- [30] B. J. Frey and D. Dueck, "Clustering by passing messages between data points," *Science*, vol. 315, no. 5814, pp. 972–976, 2007.
- [31] B. Morris and M. Trivedi, "Learning trajectory patterns by clustering: Experimental studies and comparative evaluation," in *Computer Vision and Pattern Recognition, 2009. CVPR 2009. IEEE Conference on*. IEEE, 2009, pp. 312–319.
- [32] J.-G. Lee, J. Han, and K.-Y. Whang, "Trajectory clustering: a partition-and-group framework," in *Proceedings of the 2007 ACM SIGMOD international conference on Management of data*. ACM, 2007, pp. 593–604.